Atmospheric Research 299 (2024) 107160

Contents lists available at ScienceDirect

Atmospheric Research

journal homepage: www.elsevier.com/locate/atmosres

Spatial-temporal variations and drivers of the compound dry-hot event in China

Yanjun Hu [a], Wen Wang [a,*], Peng Wang [b], Adriaan J. Teuling [c], Ye Zhu [d]

[a] National Key Laboratory of Water Disaster Prevention, Hohai University, Nanjing, China
[b] School of Ecology and Environment, Hainan University, Haikou, China
[c] Hydrology and Quantitative Water Management Group, Wageningen University and Research, Wageningen, the Netherlands
[d] School of Hydrology and Water Resources, Nanjing University of Information Science and Technology, Nanjing, China

ARTICLE INFO

Keywords:
Compound extreme event
Drought
Heatwave
Land-atmosphere coupling

ABSTRACT

Compound extremes such as compound dry-hot events (CDHEs) have received more attention in the last decade due to their more devastating impacts than those caused by droughts or heatwaves separately. A daily-resolution CDHE index, i.e., compound dry-hot index daily (CDHId), based on the copula and conditional probability is proposed to identify dry and hot days to quantify the CDHE severity. Standardized precipitation index (SPI), standardized temperature index (STI), and CDHId are used to explore the spatial-temporal variations of droughts, heatwaves, and CDHEs in China from 1961 to 2020. Results show that CDHEs occurred more frequently after the period from the late 1970s to the early 1980s. Northeast China, Southwest China, and the Tibetan Plateau witnessed the most significant increases in CDHEs. CDHEs are further classified into two types based on the sequential order of the drought and heatwave occurrence, and the drought-preceded CDHEs accounted for 85.2% of all events, indicating that CDHEs were more likely to be induced by antecedent dry conditions. Stronger land-atmosphere coupling was observed both prior to and during CDHEs compared to periods under non-dry-hot conditions, which played a major role in the formation of CDHE at the local and short-time scale. However, the annual variation of CDHE frequency in multi-decades was dominated by heatwaves, with a more significant direct path coefficient than droughts over China. Overall, the increase and enhancement of CDHEs since the early 1980s were consistent with global warming.

1. Introduction

Global warming has aggravated weather and climate extremes over the past decades all around the world. Compound extreme events were defined broadly as the combination of multiple drivers and/or hazards that contribute to societal or environmental risk (Zscheischler et al., 2018), and have attracted more attention due to their larger impacts compared to individual extremes. Compound dry and hot events (CDHEs) are among the most impactful compound events that can have adverse effects on human health and ecological systems (He et al., 2022; Libonati et al., 2022; Osman et al., 2022). CDHE is generally defined as a period during which extreme dry and hot conditions occur concurrently and consecutively, ranging in duration from pentads to seasons (Mo and Lettenmaier, 2015; Zscheischler and Seneviratne, 2017). Even over a short span of a few days, CDHEs can contribute to the exacerbation of wildfires and ecological loss (Ruffault et al., 2020). Significant increasing and widespread trends of CDHEs have been observed in China over the past decades (Wu et al., 2019; Ye et al., 2019; Yu and Zhai, 2020).

Numerous studies have explored CDHEs using diverse identification methods based on different indices and timescales. In some research, droughts and heatwaves are independently identified using respective indices, and the overlapping period of the two extreme events is identified as a CDHE (Mazdiyasni and AghaKouchak, 2015; Li et al., 2019; Feng et al., 2021). Although this method is straightforward and precise, it overlooks the dependence between dry and hot conditions (Zscheischler and Seneviratne, 2017). By constructing a joint distribution function, multiple factors such as precipitation and temperature can be integrated to develop a bivariate index (Li et al., 2021; Zscheischler and Seneviratne, 2017). For example, Hao et al. (2020) proposed a monthly CDHE index (CDHI) using copula models to quantify CDHEs in Texas. However, since heatwaves often evolve over a few days to a week

* Corresponding author at: National Key Laboratory of Water Disaster Prevention, Hohai University, Nanjing 210000, China.
E-mail address: wangwen@hhu.edu.cn (W. Wang).

https://doi.org/10.1016/j.atmosres.2023.107160
Received 18 April 2023; Received in revised form 25 November 2023; Accepted 4 December 2023
Available online 7 December 2023
0169-8095/© 2023 Elsevier B.V. All rights reserved.

(Perkins and Alexander, 2013), the monthly resolution may be too coarse for capturing short-term heatwave events effectively. A similar index called standardized compound drought and heat index (SCDHI) was then introduced at a daily resolution (Li et al., 2021). Since these two indices do not impose specific constraints on dry and hot conditions individually, some dry-cold or wet-hot events may be incorrectly identified as CDHEs.

Across the scale of days to multi-years, there are two main physical mechanisms contributing to the onset, evolution and intensification of CDHEs, i.e., persistent atmospheric processes and land-atmosphere feedbacks (Miralles et al., 2019; Zhang et al., 2021). At a large scale, some persistent circulation patterns are responsible for the initiation of both droughts and heatwaves, including but not limited to subtropical highs, blocking highs and atmospheric stagnation events (Hao et al., 2018; Zhang et al., 2021). At the regional scale, the land-atmosphere (L-A) feedback also plays a significant role in the occurrence and exacerbation of CDHEs (Gallego-Elvira et al., 2016; Stéfanon et al., 2014; Vicente-Serrano et al., 2014). A shortage of precipitation (P) and soil moisture (SM) deficiency result in an increased partitioning of energy towards sensible heat, subsequently leading to a temperature (T) increase (Hirsch et al., 2019). On the other hand, T increase elevates atmospheric water demand and further depletes SM, which is unfavorable for rainfall, resulting in intensified drought (Miralles et al., 2019). Seo and Ha (2022) investigated the soil moisture-temperature coupling strength over northern East Asia and found that the L-A coupling enhanced the CDHEs. Zhang et al. (2019) took the actual evapotranspiration (AET) anomaly as the primary criterion for classification, defining CDHEs with AET $>$ 0 as high-temperature-induced compound events and those with AET $<$ 0 as drought-induced events. However, the response of AET to T increases is nonlinear and highly dependent on local ecosystem conditions (Budyko, 1961). For example, in arid and semi-arid regions, AET is negatively correlated with potential ET under water-limited conditions (Han et al., 2014), which implies that despite increasing T, AET would still diminish due to an inadequate supply of water available for evaporation. Though several studies have demonstrated that the L-A feedback can exacerbate CDHEs, the specific coupling mechanism prior to and during the CDHE has not been fully understood on a daily basis. By employing daily indices, it becomes feasible to investigate the land-atmosphere coupling processes at a daily resolution, which have been observed to occur within a few days (Teuling et al., 2006).

Regarding the dominant driver of the temporal variation of CDHE in multi-decades, Vogel et al. (2021) found that the rise in the number of CDHEs in the Mediterranean Basin was primarily driven by temperature changes but not precipitation, and suggested that CDHE changes may be dominated by heatwaves. Also, Zhang et al. (2022) suggested that temperature was the dominant factor influencing CDHEs globally in the past (1951–2014), and CDHEs will be sensitive to global warming in the future. However, Bevacqua et al. (2022) stated that the future frequency of dry-hot extreme events is primarily determined not by temperature trends, but by precipitation. To date, although the spatial-temporal characteristics of CDHEs have attracted more attention, there remains relatively scarce analysis regarding their long-term driving factors in China.

To accurately quantify CDHEs, a daily compound dry-hot index (CDHId) is proposed in Section 2. In Section 3, SPI, STI, and CDHId are used to identify and evaluate the variations of droughts, heatwaves, and CDHEs in China during 1961– 2020; the CDHEs are further classified into two types based on the sequential order of the drought and heatwave occurrence. At the regional scale, the land-atmosphere (L-A) feedback both prior to and during two types of CDHEs are statistically investigated using two L-A coupling indices. For decadal variations, we quantitatively analyze the dominant factor (either drought or heatwave) influencing long-term changes in CDHEs through path analysis. The analyses are expected to provide an in-depth insight into dry and hot extremes in China and would be helpful for climate change adaptation and mitigation.

2. Materials and Methods

2.1. Data used

Due to the vast territory and diverse topography, the climate in China varies from the subtropical zone in the south to the cold temperate zone in the north. The Tibetan Plateau has an alpine climate and far inland regions in the northwest are mostly very dry. For the convenience of describing the changes in different regions, we divide mainland China into 6 sub-regions, Northwest China (NW), Central North China (CN), Northeast China (NE), Tibetan Plateau (TP), Southwest China (SW), and Southeast China (SE), according to administrative districts and climate zones (see Fig. 1).

Gridded daily precipitation (P) and daily maximum temperature (T) data during 1961–2020 are obtained from the China Ground Precipitation/Temperature Daily 0.5° × 0.5° Gridded Dataset (V2.0) at the National Meteorological Information Center (2012; http://www.nmic.cn/). These datasets were resampled from ground observation station data, and have undergone cross-validation and error analysis. Data from the China Meteorological Forcing Dataset (Chen et al., 2011; Yang and He, 2016) and the China Land Data Assimilation System (http://data.cma.cn/data/cdcdetail/dataCode/NAFP_CLDAS2.0_NRT.html; Shi et al., 2014) are used to fill in the missing data. The gridded data are developed based on over 2000 ground-based national meteorological stations (http://www.nmic.cn/; there is no data in the Taiwan region). The number of meteorological stations in each 0.5° × 0.5° grid cell is indicated in Fig. 1. The density of stations used for generating the gridded data is relatively high in the eastern part of China, while low in the western part of China (especially in Xinjiang and the western part of the Tibetan Plateau), which makes the data less reliable.

In addition, data of 2 m mean temperature, 2 m dewpoint temperature, latent heat flux (LH) and volumetric soil water (0-100 cm; SM) from 1961 to 2020 are retrieved from the ERA5-Land hourly 0.1° dataset (Muñoz-Sabater et al., 2021), and subsequently aggregated to daily values at 0.5°. According to the National Specifications for Surface Meteorological Observation (GB/T 35221–2017), the daily boundary for meteorological observations in China is 20:00 Beijing time (UTC + 8). Thus, the daily aggregation period starts from 20:00 Beijing time the previous day to 20:00 Beijing time the current day when aggregating ERA5-Land hourly data to the daily data. The vapor pressure deficit (VPD) is estimated using the 2 m mean temperature and dewpoint temperature.

2.2. Identification of droughts and heatwaves

The standardized precipitation index (SPI) is among the most commonly used indices for meteorological drought identification. To calculate the SPI, the cumulative precipitation data are often assumed to follow a gamma distribution and then transformed to the standard normal distribution by applying the inverse normal function (McKee et al., 1995). The cumulative precipitation is usually calculated on a monthly or annual basis, but can also be calculated at a daily temporal resolution so as to provide details of the drought development process (Stagge et al., 2015). According to the investigation of Wang et al. (2021), a 90-day timescale SPI is suitable for assessing meteorological drought in different climate regions over China. In this study, SPI is calculated using cumulative precipitation in a moving window of 90 days on a daily basis (unless otherwise specified, the SPI hereafter refers specifically to the 90-day timescale SPI). In general, droughts are typically identified as having a minimum duration of one month. However, in recent years, shorter-duration events known as flash droughts have been widely observed and proven to have significant impacts (Otkin et al., 2018; Yuan et al., 2023). In this paper, a meteorological drought event is identified if the daily SPI $\leq$ -1 for at least 20 consecutive days.

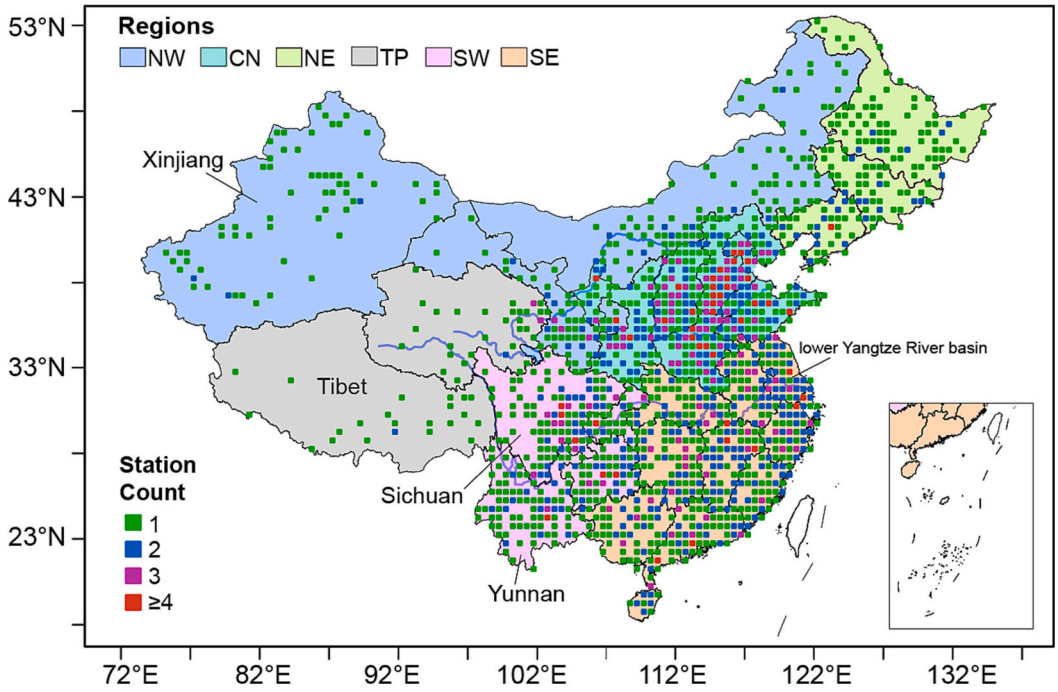

Fig. 1. Sub-regions and the number of meteorological stations in each 0.5° × 0.5° grid cell over mainland China.

Two adjacent drought events are merged as one drought event if the time interval between the two preliminary events is no >5 days with SPI ≤ 0 during the interval.

Assuming that the daily maximum temperature follows the normal distribution, the daily maximum temperature is normalized to construct the standardized temperature index (STI) as follows (Zscheischler et al., 2014):

$$\mathrm{STI(i)} = \frac{T(\mathrm{i}) - T_{\mu}}{T_{\sigma}} \tag{1}$$

where T_{μ} and T_{σ} refer to the mean and standard deviation of the daily maximum temperature series, which is constructed from the daily maximum temperature of a 31-day window centered on the day i in each year. A heatwave is preliminarily identified if STI ≥ 1 in at least 5 consecutive days, and two preliminary heatwaves are merged if they have an interval ≤ 3 with STI ≥ 0 during the interval.

2.3. Identification and characterization of CDHE

In this study, the CDHE is defined as a period of at least 10 consecutive days during which both dry and hot anomalies occur simultaneously (SPI ≤ -1 and -STI ≤ -1). A day when both SPI and -STI break the threshold (−1) is identified as a dry-hot day. The copula function is used to estimate the occurrence probability and quantify the severity of those dry-hot days in the present study. Copulas are great tools for modeling and simulating correlated random variables so as to examine the dependence between many variables. Here, the copula function is used to link SPI and STI to construct an index on a daily basis, i.e., the compound dry-hot index daily (CDHId). The detailed process for calculating CDHId is as follows:

1. Calculate the daily SPI and STI and their correlations. If they show a significant correlation (at the 0.05 significance level), the joint distribution function can be constructed from a copula function.
2. Select the preferred copula function and obtain the joint distribution. Assuming two random variables X and Y, representing SPI and -STI respectively (for the convenience of the probability calculation, we set Y = -STI), the marginal distributions can be denoted by U(x) = ϕ(x) and V(y) = ϕ(y) since both X and Y follow the standard normal distribution. Here, we consider various copula models, including the Gaussian copula and three commonly used copulas of the Archimedean family (Clayton, Gumbel and Frank), which have mathematical tractability and can capture varieties of dependence structures (Ganguli and Reddy, 2013). These copulas are selected as candidates for fitting the joint distribution of SPI and STI. The 'VineCopula' package in R (Nagler et al., 2021) is used to fit the optimal model based on Akaike's information criteria (AIC). Once the copula model (denoted as C) is determined, the joint distribution can be expressed as:

$$\mathrm{C(U(x), V(y))} = P(U \le \mathrm{u}, V \le \mathrm{v}) = P(\mathrm{X} \le x, Y \le \mathrm{y}) \tag{2}$$

3. Identify dry-hot days. The dry-hot days are identified under the conditions that SPI ≤ -1 and STI ≥ 1, i.e., X ≤ -1 and Y ≤ -1.
4. Calculate CDHId. For each dry-hot day (x', y'), its severity relative to the drought and heatwave thresholds (SPI = -1, STI = 1) can be expressed using the conditional probability P_0 calculated below:

$$P_0 = P(\mathrm{X} \le x', Y \le y' | \mathrm{X} \le -1, Y \le -1) = \frac{\mathrm{C}(U', V')}{\mathrm{P}(\mathrm{X} \le -1, \mathrm{Y} \le -1)} \quad (x' \le -1, y' \le -1) \tag{3}$$

where $P(\mathrm{X} \le -1, Y \le -1)$ can be estimated by the proportion of dry-hot days in total days, and P_0 represents the severity of compound dry and hot conditions relative to the drought and heatwave thresholds. A lower value of P_0 implies a more severe condition of dry and hot. In order to characterize the severity of CDHEs using the cumulative values on a daily basis during the whole duration, the CDHId is defined as CDHId = 1-P_0. The index ranges between [0,1], and the larger the value, the more extreme the CDHE condition is. The CDHId cumulative distribution exhibited a negative skew.

5. Identify compound events based on the CDHId. A CDHE is identified as a period when the CDHId>0 persists for at least 10 consecutive days. We use a minimum duration criterion of 10 days to capture

those short-term but potentially ecologically damaging CDHEs (Ruffault et al., 2020). If the interval between two adjacent events is no >3 days, and either the SPI or -STI index is consistently below −1 during the period, the two events are merged into one event. On normal days, the CDHId value remains 0. The CDHEs are investigated in the year-round period rather than only in the warm season since extremes outside the warm season also pose threats to agriculture and ecosystems, which cannot be ignored (Ben-Ari, 2018; Brás et al., 2021).

To characterize the extremes (including droughts, heatwaves and CDHEs), the following metrics are calculated at each grid (if an event spans two years, the event is only counted in the year when it starts):

(1) Frequency (F): the total number of extreme events in a year (unit: times).
(2) Duration (D): the total days of extreme events in a year (unit: days).
(3) Severity (S) of drought and heatwave: the average of the SPI and STI during events in a year, expressed as follows:

$$S = \begin{cases} \dfrac{\sum_{i=1}^{D} I_i}{D} \text{ (when } I \text{ refers to STI)} \\ -\dfrac{\sum_{i=1}^{D} I_i}{D} \text{ (when } I \text{ refers to SPI)} \end{cases} \quad (4)$$

where I_i refers to the index (SPI or STI) of the ith day in the whole duration of a year. When I refers to the SPI, the S is made negative so that the signs of S give a consistent indication of the severity for droughts and heatwaves (i.e., the higher the S, the more severe the dry/hot condition).

(4) Coverage (A): the ratio of the area where extreme events occurred (i.e., frequency F ≥ 1) during a year to the total area of the study area (unit: %).
(5) Magnitude (M) of CDHE: the sum of the indices during CDHEs in a year:

$$M = \sum_{i=1}^{D} CDHId_i \quad (5)$$

To get annual areal averages of those metrics over China, the area-weighted averages are calculated considering the size of grid cells.

2.4. CDHE Classifications

With the usage of daily indices, it is intuitive to investigate the triggering factor of CDHEs by distinguishing the sequential order of the drought and heatwave. We further define two types of CDHEs, that is, (a) drought-preceded CDHE ($CDHE_d$): the CDHE with a drought occurs first; (b) heatwave-preceded CDHE ($CDHE_h$): the CDHE with a heatwave occurs first. The indicator used to identify these two types of events here is the dry-hot lag (Δd), which is the time difference between the onset of the drought and that of the heatwave involved in a CDHE, given by:

$$\Delta d = d_2 - d_1 \quad (6)$$

where d_1/d_2 is the first day of a drought/heatwave. A CDHE with a positive Δd refers to the drought-preceded CDHE ($CDHE_d$), indicating that the drought occurs before heatwaves, while a negative Δd refers to a heatwave-preceded CDHE ($CDHE_h$).

The proportions of $CDHE_d$, i.e., the $CDHE_d$ frequency (F_{CDHEd}) divided by the frequency of total CDHEs (F_{total}) at each grid are calculated. The higher the proportion, the greater the possibility of drought-preceded CDHEs occurrence at the grid.

2.5. Land-atmosphere coupling index

The land-atmosphere (L-A) coupling is investigated by the terrestrial coupling index and atmospheric coupling index (Dirmeyer et al., 2013; Hirsch et al., 2019), which are calculated as:

$$I_T = \frac{COV(SM_{scaled}, LH_{scaled})}{\sigma_{SM_{scaled}}} \quad (7)$$

$$I_A = \frac{COV(VPD_{scaled}, LH_{scaled})}{\sigma_{LH_{scaled}}} \quad (8)$$

where *SM_scaled*, *LH_scaled* and *VPD_scaled* denote the soil moisture, latent heat flux and vapor pressure deficit, respectively, each normalized through z-score standardization; σ denotes the standard deviation (approximately 1); $COV(a, b)$ is the covariance between a and b. The physical meaning of I_T (I_A) is the change in LH (VPD) caused by a one-unit change in SM (LH). A positive I_T indicates that the LH decreases together with SM, responding to a water-limited regime; a negative I_T indicates the LH increases despite a decrease in SM, suggesting that there is an energy-limited regime (Hsu and Dirmeyer, 2022).

For each CDHE occurred from the kth to mth day of the year i ($Day^i_{k\sim m}$), the coupling indices are calculated in three periods separately: (a) 10-days prior to the onset of the CDHE ($Day^i_{k-10\sim k-1}$); (b) during the CDHE ($Day^i_{k\sim m}$); (c) the counterpart period in each year ($Day^{1961\sim2020}_{k\sim m}$). These three periods are selected for assessing the L-A coupling characteristics before/during CDHEs and under normal circumstances.

2.6. Evaluation of the temporal changes of dry and hot events

The piecewise linear fitting model (PLFIM) is a statistical method that utilizes linear regression to model temporal series divided into several intervals, with breakpoints selected using the least-squares method to determine the best fit, which has been widely employed to investigate the change point of long-term linear tendencies of diverse climate parameters (Tomé and Miranda, 2004). In this paper, PLFIM was applied to detect the shifts assuming that there is only one single breakpoint with trends in different directions before and after the breakpoint. The data length before and after the breakpoint should be at least ten years. In addition, we applied F-test to test the significance of the linear trend. If the p-value<0.05 for at least one segment, the breakpoint is considered to be significant at the significance level of $\alpha = 0.05$. If no breakpoint is detected, the Mann-Kendall trend test (MK test; Kendall, 1955; Mann, 1945) and linear regression will be applied to the whole series to assess the significance of the overall trend. The MK test calculates the Kendall rank correlation coefficient (Kendall's τ) between the time series and time, which is a statistic measuring the strength of the monotonic trend and taking values between [−1,1]. A positive Kendall's τ indicates an increasing trend in the time series, while a negative one indicates a decreasing trend.

$$\begin{cases} r_{1z} = P_{z1} + r_{12}P_{z2} \\ r_{2z} = P_{z2} + r_{12}P_{z1} \end{cases} \quad (9)$$

where r_{ij} (r_{iz}) is the Pearson correlation coefficient of x_i and x_j (z); P_{zi} is the direct path coefficient of x_i on z, indicating the direct effect from x_i to z; $r_{12}P_{zj}$ is the indirect path coefficient from x_i to z through x_j. The direct path coefficient represents only the direct effect of x_i (drought and heatwave) on z (CDHE), excluding any indirect or mediated effects through other variables.

The path analyses were performed at each sub-region and over China, using the package 'lavaan' in R (Rosseel, 2012). All results of path analysis presented in this paper have a standardized root mean squared residual (SRMR) <0.1, indicating a good fit for the model. R-squared (R^2) was provided to reflect the proportion of variance in z that is explained by x_1 and x_2.

3. Spatial and temporal variations of droughts, heatwaves, and CDHEs

3.1. Negative relationships between P and T

When building a Copula model for two variables, a dependent relationship between the two is the prerequisite, thus firstly we calculate the Pearson correlation coefficients between SPI and STI. Fig. 2 illustrates the spatial distribution of the correlation coefficients over China in different seasons. In general, significant (at the 0.05 level) negative correlations prevail in the majority of the nation all year round. In spring and summer, there are stronger negative P-T correlations, with negative correlations observed in 99.8% and 98.7% of areas, respectively, compared to autumn and winter (where negative correlations were observed in 84.6% and 88.4% of areas). In eastern China, the correlation is generally higher during the summer compared to the spring season. Conversely, in western regions, especially in western Xinjiang, the opposite pattern is observed, with a higher correlation during spring than in summer. Since the correlations are significant in most areas, the joint distributions are constructed for the whole region.

3.2. Characteristics of CDHId

Several multivariate indices have been proposed for identifying CDHEs in the literature to avoid the limitations of traditional univariate methods, such as the CDHI (Hao et al., 2020) and the SCDHI (Li et al., 2021). However, both of these two indices have no constraints on the dryness or hotness when constructing joint distribution for SPI and STI, leading to the identification of dry-cold (SPI < 0, STI < 0) or wet-hot (SPI > 0, STI > 0) situations. Here we illustrate the effectiveness of CDHId for avoiding such issues, taking a randomly selected grid cell at 96° 45′ E, 39° 15′ N as an example.

The scatter plot of joint probability calculated with Eq. (2) about the relation of SPI (X) and -STI (Y) at the cell is shown in Fig. 3a. Note that only days with a joint cumulative probability below 0.3 were presented. Results suggest that, though the joint probability successfully quantifies the severity of CDHEs (lower probability indicates more severe conditions), conditions like dry-cold and wet-hot cannot be ruled out relying on the value of joint probability alone. For instance, the orange cross signs which indicate days that compose a CDHE during the period from 30 August to 7 October 2016 according to their joint probability are actually quite normal in temperature (i.e., STI < 0, see Fig. 3b). On the other hand, the pink plus signs indicate a CDHE from 27 January to 5 February 2007, with SPI > 0 for all the time, which is clearly not in a

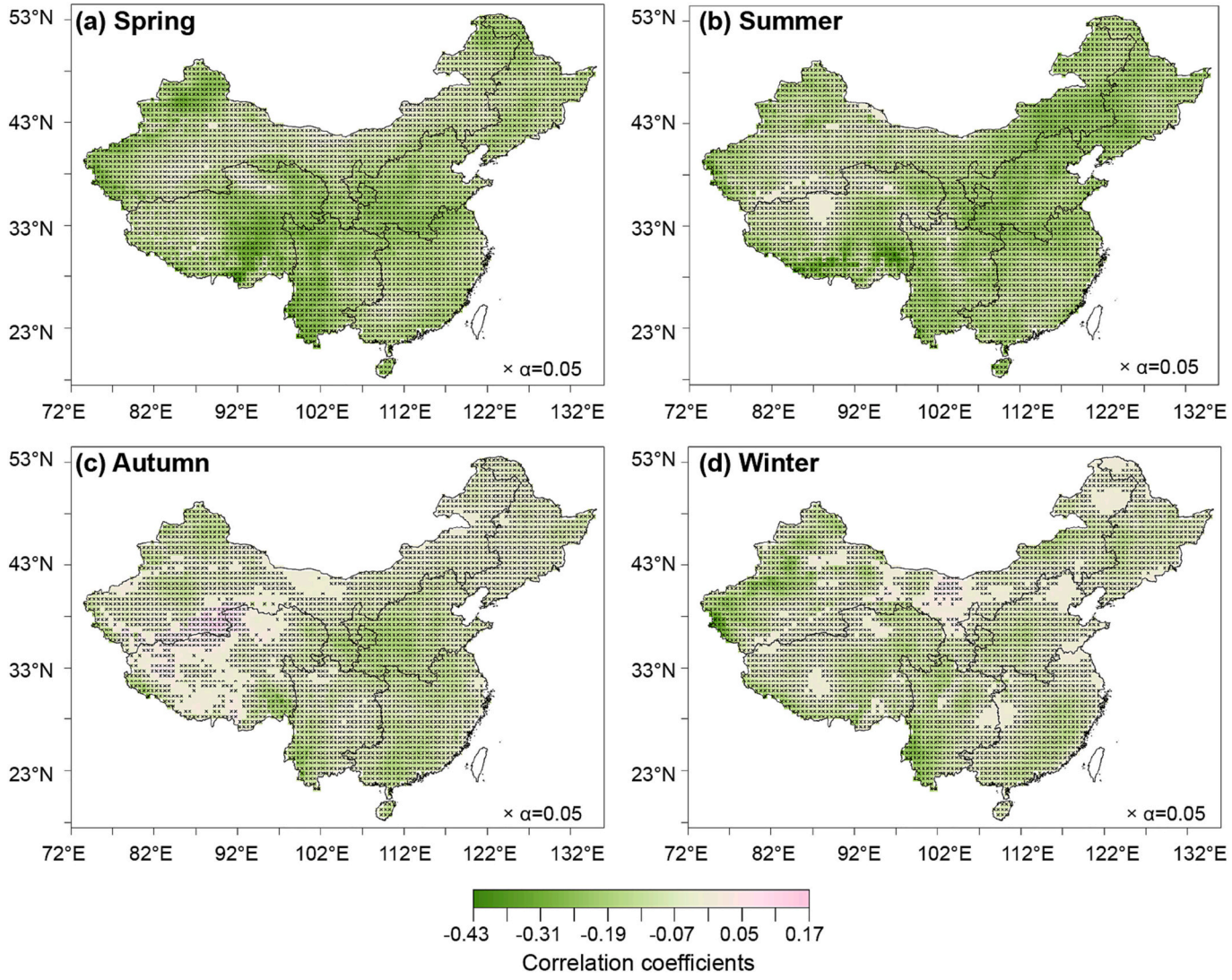

Fig. 2. Pearson correlations between daily SPI and STI during (a) spring, (b) summer, (c) autumn and (d) winter in 1961–2020. The cross denotes that the correlation is significant at the 0.05 level.

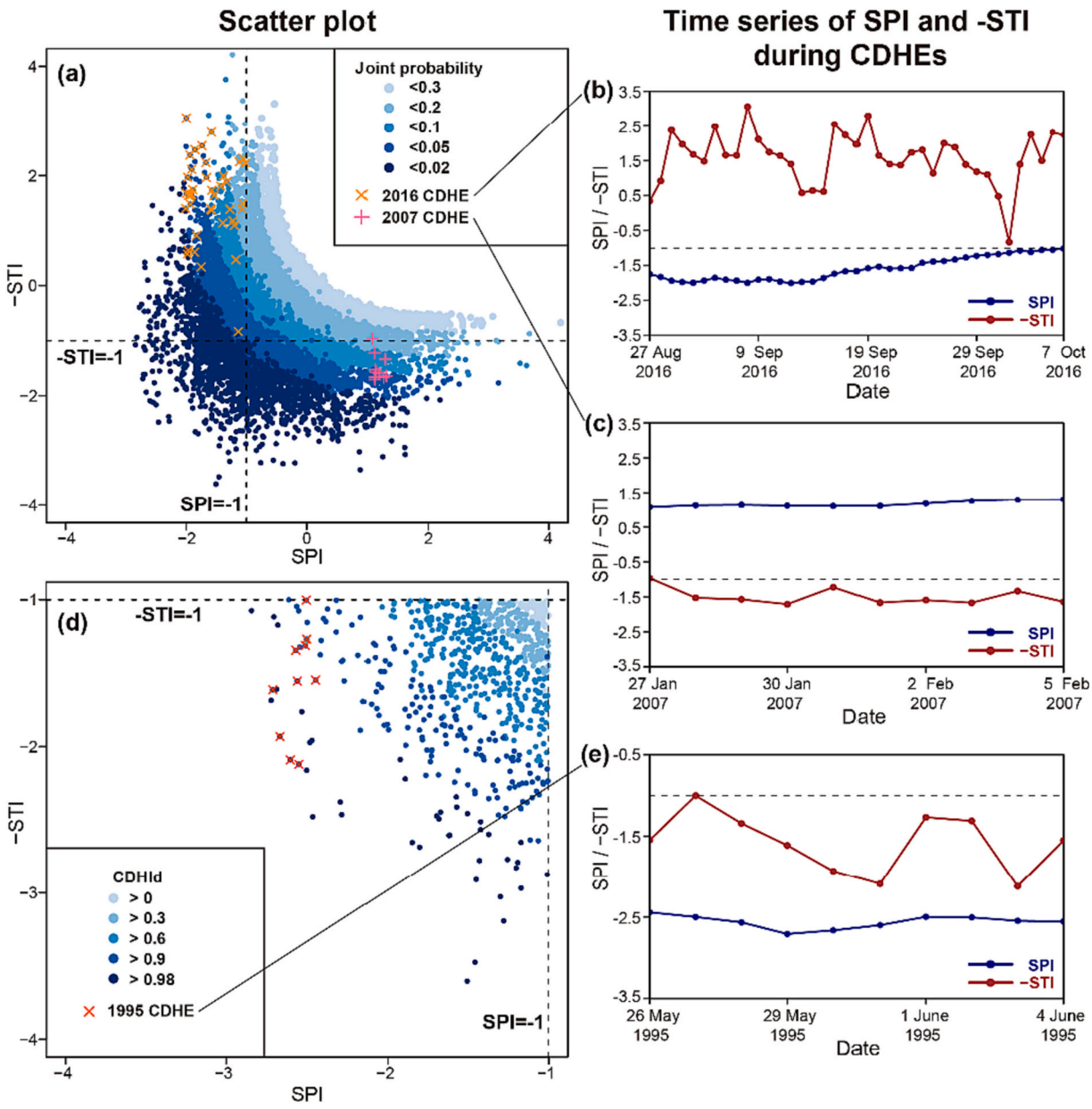

Fig. 3. The scatter plots of the SPI and STI at the example cell centered at 96° 45′ E, 39° 15′ N during 1961– 2020. The group of crosses and plus signs indicate CDHEs identified by (a) the joint probability without individual limits for dry and hot conditions, and (d) CDHId. The corresponding processes of SPI and -STI in CDHEs are shown in (b), (c), and (e), where blue lines represent SPI, red -STI. (For interpretation of the references to colour in this figure legend, the reader is referred to the web version of this article.)

drought situation (see Fig. 3c). Such excessive identification is common in other cells all over China when using indices based on joint probability without setting individual conditions for variables, and would lead to overestimation of the frequency of CDHEs, whereas CDHId avoids such problems by adding the conditional probability. For the same cell, dry-hot days identified by CDHId are revealed in Fig. 3d. Possible events are constrained in the space with SPI < -1 and STI > 1, thus non-extreme conditions such as those shown in Fig. 3b and Fig. 3c are excluded. Restricted by the criterion of temporal continuity (10 days), only one CDHE that occurred from 26 May to 4 June 1995 (represented by the red crosses in Fig. 3d, the corresponding progress in Fig. 3e) is identified among all dry-hot days.

3.3. Temporal changes of droughts, heatwaves, and CDHEs

The annual areal averages of the frequency, duration, severity (for droughts and heatwaves), magnitude (for CDHEs) and coverage of droughts, heatwaves and CDHEs over China during 1961– 2020 are presented in Table 1. The variations for the average frequency (F), duration (D), Severity (S) of droughts and heatwaves, magnitude (M) of CDHEs, and Coverage (A) of droughts, heatwaves, and CDHEs,

Table 1
The annual areal averages of characteristics of droughts, heatwaves, and CDHEs in China from 1961 to 2020.

Events	Frequency (times)	Duration (days)	Severity (for droughts and heatwaves) /Magnitude (for CDHEs)	Coverage (%)
Droughts	0.74	39.77	0.88	26
Heatwaves	2.39	17.19	1.38	86
CDHEs	0.07	1.02	0.83	6

respectively, over the whole mainland China and/or different regions during 1961– 2020, are presented in three columns in Fig. 4. We conducted the PLFIM to detect the breakpoint for each series and calculate the linear trends before and after it; the MK test and linear regression were employed to assess the overall trend and the change rate if there was no significant breakpoint.

As illustrated in column (a) in Fig. 4, the frequency of droughts showed a significant downward trend at a rate of −0.04 times/decade. The duration and severity of drought both showed overall negative trends based on the Mann-Kendall (MK) test and the linear regression. The coverage also decreased significantly ($\alpha = 0.05$) at a rate of −1.7% per decade. Generally, the drought in China got less frequent, shorter, and less severe. Column (b) in Fig. 4 presented upward trends in frequency and duration (increased by 0.05 times/year and 0.44 days/year, respectively) of heatwaves since 1976. The severity exhibited similar change patterns but broke in 1983. As for coverage, heatwave events covered more areas in China since the 1970s. At the national average level, the heatwave decreased in frequency and severity before the late 1970s or the early 1980s, but increased in frequency, duration, severity, and coverage afterwards, especially since the 1990s. Regarding the CDHE shown in column (c) of Fig. 4, there has been a common increasing trend in its frequency, duration, severity, and coverage across all regions of China since the 1970s. Although the CDHE reached its peak in 1963, with frequency, duration and magnitude all being the highest, it experienced a period of low levels during the 1970s to the 1990s and became more frequent and severe after the end of the 1990s.

Some studies suggest that heatwaves have become more frequent and severe across China since the 1990s (Xie et al., 2020; Ding and Ke, 2015), which is much later than the breakpoint of the 1970s detected in this study. The major reason for the difference is the type of breakpoint. Breakpoints may exist in the mean, variance or trend in a time series. In the aforementioned studies, the breakpoints in the 1990s were detected based on the distributions and mean values. In our study, the PLFIM is applied to detect breakpoints in trends. The detected breakpoint in trends would occur earlier than the breakpoint of the mean value because the change of trend would not affect the mean value much until there is a substantial accumulation of trend changes.

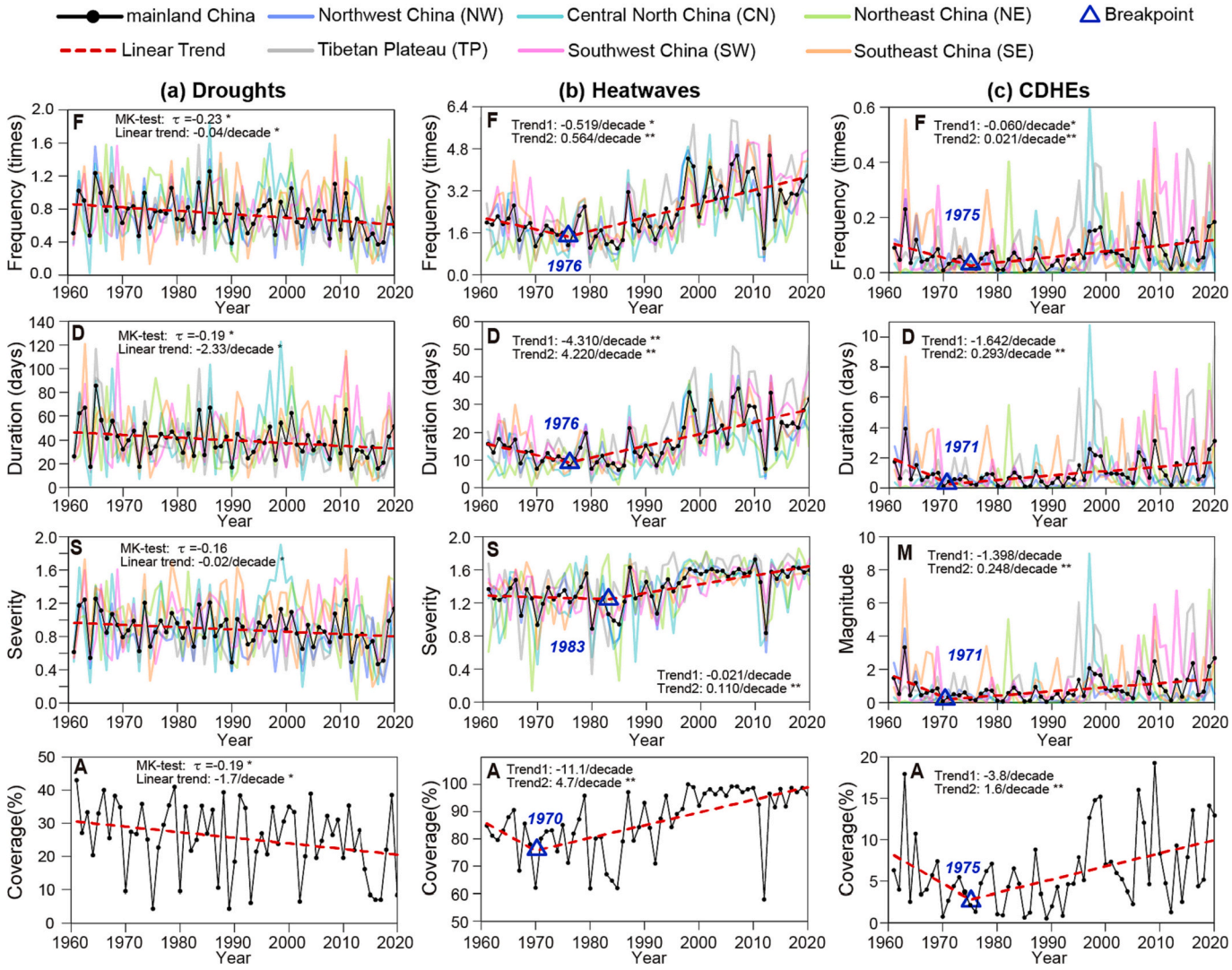

Fig. 4. Variations of the average frequency (F), duration (D), Severity (S) (of droughts and heatwaves)/magnitude (M) (of CDHEs), and Coverage (A) of (a) droughts, (b) heatwaves, and (c) CDHEs, respectively in three columns, over the whole mainland China and/or different regions during 1961– 2020. Breakpoints were detected by the piecewise linear fitting model (PLFIM) and denoted by blue triangles. For the series without significant breakpoints, the MK test and the linear regression were applied. The red dash lines denote the linear trends for the time series segment before (Trend1) and after (Trend2) the breakpoints, or for the whole series. The asterisks denote the trend is significant at the 0.05 level (*) or the 0.01 level (**). (For interpretation of the references to colour in this figure legend, the reader is referred to the web version of this article.)

3.4. Spatial distribution of changes in droughts, heatwaves, and CDHEs

To examine the spatial patterns of CDHE changes, the PLFIM and MK tests were performed in each region. Fig. 5 illustrates the MK trend at each grid and region during the time period from 1961 to 2020. Note that, as the four characteristics (i.e., F, D, S and M) showed consistency in their temporal variations (see Fig. 4), only the frequency (F) for droughts and heatwaves and magnitude (M) for CDHEs were presented to save space.

Regionally, drought frequency in NW and TP decreased significantly in the whole period (Kendall's τ equals -0.22 and -0.33, with p-values<0.05). In SE, CN and NE, droughts decreased slightly (τ less than -0.10, p-value>0.05). There was a discernible belt extending from the western part of NE to SW (especially in Yunnan Province), which presented an increasing trend in droughts. Most parts in SW and small parts of southern TP experienced significant increases in frequency. The spatial distribution of trends during the whole period presented in Fig. 5 (b) exhibited a nationwide increase in heatwave frequency. The increasing trends were strong except for the western and northern Xinjiang, eastern NE, small areas in Sichuan province and southern CN. As for CDHEs, overall significant increases in CDHE magnitude were observed in NE and SW, with SW exhibiting the most severe increases ($\tau = 0.33$). Only 17% of areas of the nation exhibited significant decreases in CDHE magnitude, including northern Xinjiang and lower reaches of the Yangtze River basin.

3.5. Characteristics and typical processes of two types of CDHEs

To investigate potential triggering factors of CDHEs, we compared the sequence of drought and heatwave occurrences within each event and calculated Δd according to eq. (6). The density histogram of Δd for CDHEs across all grids from 1961 to 2020 is presented in Fig. 6a. The larger the positive Δd is, the longer it indicates the lead time of drought before the heatwave. In 5.0% of the CDHEs, Δd falls within the range of 100 to 391 days, representing exceptional cases linked to long-lasting droughts. To highlight the details of regular situations, values of Δd exceeding 100 days are not displayed in the histogram. Among all CDHEs, 85.0% of cases have $\Delta d > 0$, with an average leading time of 32 days. In 10.4% of events, heatwave precedes drought ($\Delta d < 0$), with an average leading time of 4.2 days. Additionally, 4.6% of cases have Δd equal to 0, suggesting the simultaneous onset of drought and heatwaves on the same day. Furthermore, events with Δd within the range of ± 5 days account for 25.5% of the total. Based on the Δd, CDHEs were categorized into two types: drought-preceded CDHEs ($CDHE_d$, $\Delta d > 0$) and heatwave-preceded CDHEs ($CDHE_h$, $\Delta d < 0$). The proportion of $CDHE_d$, i.e., the $CDHE_d$ frequency (F_{CDHEd}) divided by the frequency of total CDHEs (F_{total}) at each grid is illustrated in Fig. 6b. It is evident that the $CDHE_d$ prevailed all across China, with an average proportion of 85.2%. Only in scattered areas of TP, NW, and NE, the heatwave occurs before drought within a CDHE more frequently.

To better understand the onset and evolvement of different types of CDHEs and facilitate the verification of CDHId, we present the processes of SPI, STI, CDHId and anomalies in VPD, SM and LH of four typical CDHEs in different regions in Fig. 6c-f. Fig. 6c and e both represent typical drought-preceded CDHEs ($CDHE_d$). Before the onsets, the mean VPD anomaly remained positive, indicating higher atmospheric water demand; the SM was already deficit due to the prior droughts; the actual evapotranspiration (in another form of LH) in this period was at the average level in case (c) and notably lower in (e). During the CDHEs, VPD continued to increase, SM further decreased, and LH remained consistently low, possibly due to insufficient SM available for evapotranspiration. In Fig. 6f, despite having SM in a deficit state, the SM was not depleted during the preceding drought, which is related to its location in a relatively humid region (SE); consequently, during the CDHE, LH continued to rise due to the high temperature; the VPD did not show significant elevation in the prior drought period, but began to rise

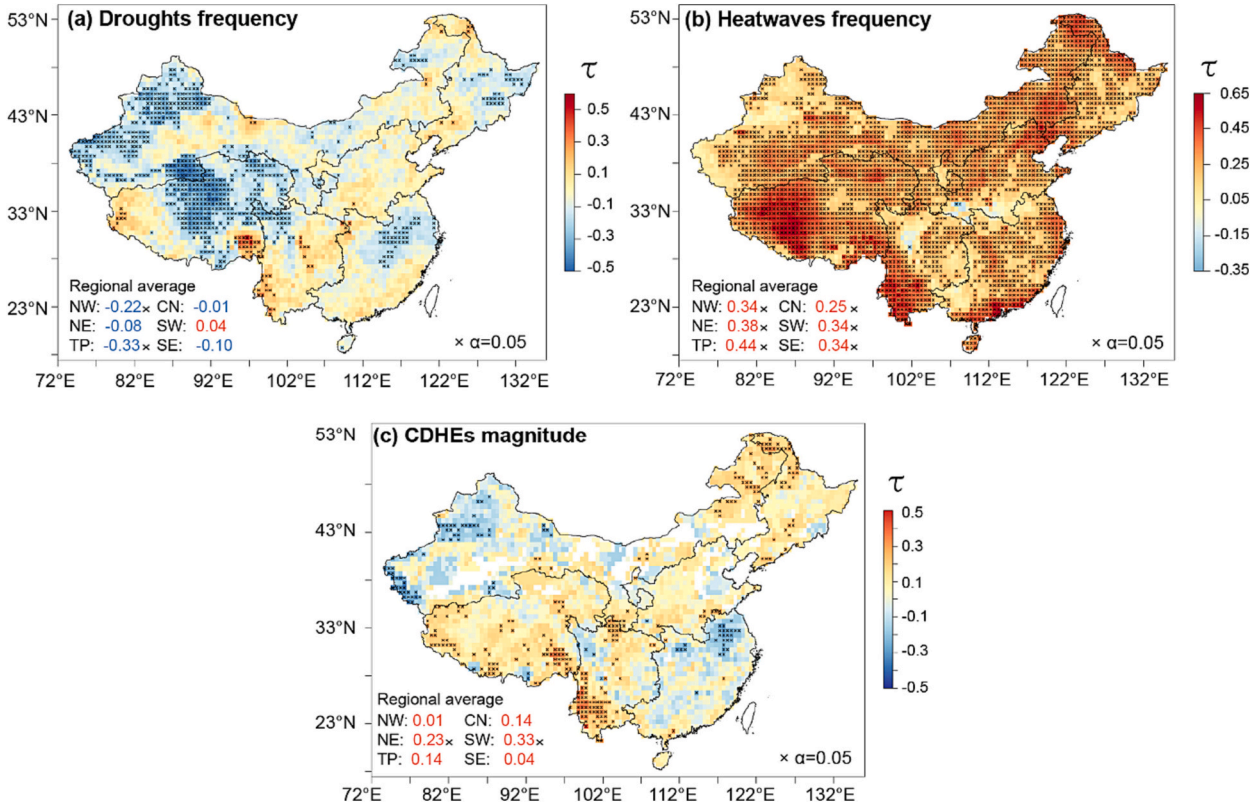

Fig. 5. MK trends of the frequency of droughts (a), heatwaves (b) and the magnitude of CDHEs (c) over China. The cross sign indicates the trend is significant at the 0.05 significance level. The blank grid indicates that there are insufficient events to conduct the MK test.

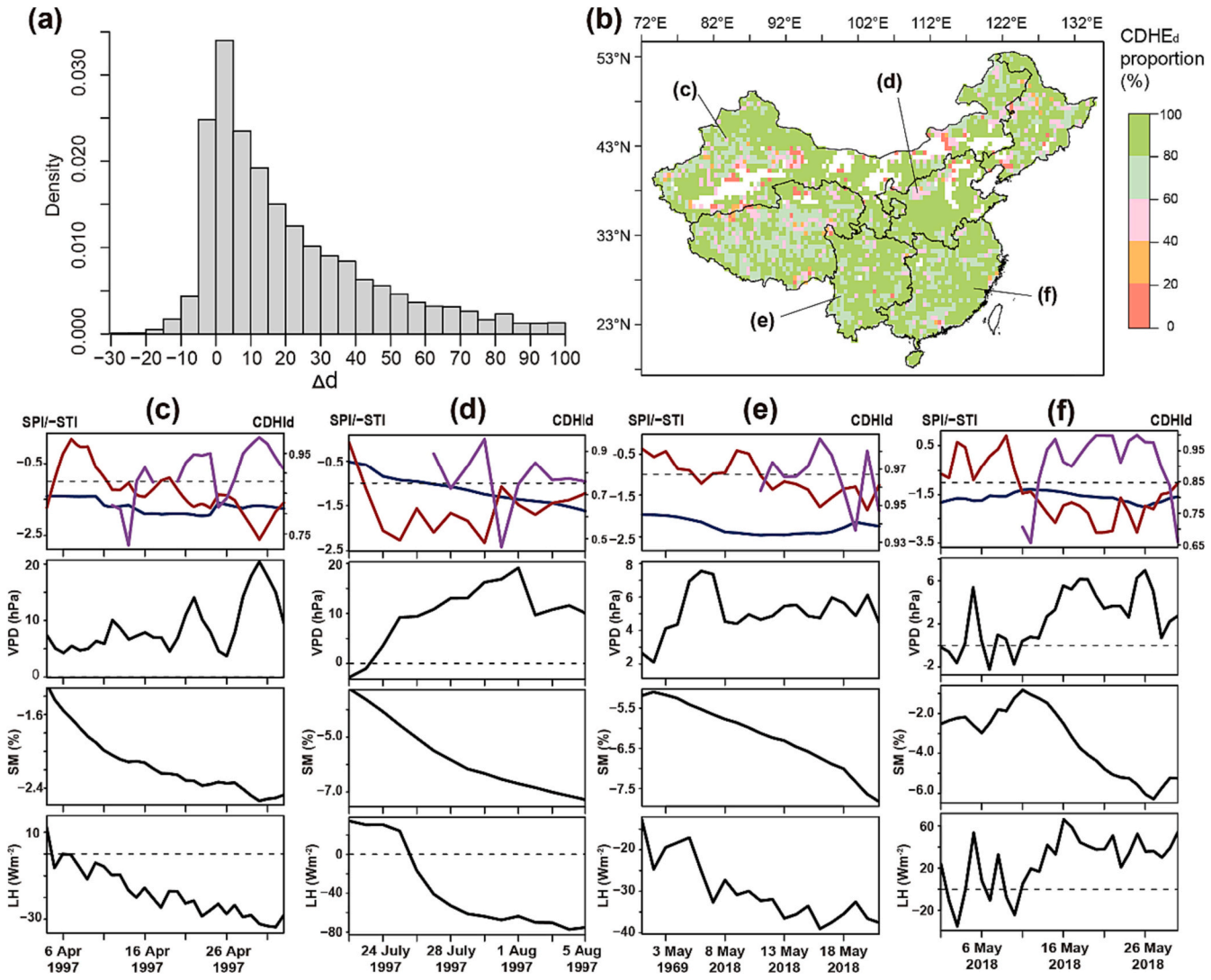

Fig. 6. Characteristics and spatial distribution of two types of CDHEs. (a) Probability histogram of Δd (only those lower than 100 days are presented). (b) Spatial distribution of the drought-preceded CDHEs ($CDHE_d$) proportion; the blank grid indicates that there are insufficient events for calculating the proportion. (c-f) Processes of SPI, -STI, CDHId and anomalies in vapor pressure deficit (VPD), soil moisture (SM) and latent heat flux (LH) during and 10-days prior to typical CDHEs in four distinct regions; the grid locations of panels c-f are all labelled in panel (b); blue lines represent SPI, red for STI, and purple for CDHId. (For interpretation of the references to colour in this figure legend, the reader is referred to the web version of this article.)

only after the onset of the CDHE. Fig. 6d represents a typical $CDHE_h$, characterized by significantly elevated VPD and LH in the antecedent heatwave; however, during the CDHE, LH decreased noticeably, possibly due to the soil moisture depletion.

3.6. Land-atmosphere coupling characteristics during CDHEs

To investigate the L-A coupling characteristics during the onset and evolution periods of CDHEs, we calculated anomalies in VPD, SM, and LH for the 10 days preceding and during each CDHE, as well as the L-A coupling indices (I_T and I_A for SM-LH and LH-VPD coupling, respectively). In addition, the coupling indices during the counterpart periods within each year were also computed to serve as a reference of the normal L-A coupling strength under non-dry-hot conditions. The statistical characteristics of these indicators for all events are depicted in the empirical probability distributions in Fig. 7.

In Fig. 7a, it is evident that the VPD already increased 10 days prior to CDHEs, with a positive VPD anomaly making up 75.9% of the total; during CDHEs, there was a substantial increase in VPD (with a positive value accounting for 96.3%). Before the event, the VPD anomaly of $CDHE_h$ (with an average of 1.3 hPa) was more severe than that of $CDHE_d$ (with an average of 1.2 hPa); however, during the event, the VPD anomaly of $CDHE_d$ (averaging 3.5 hPa) became more severe than that of $CDHE_h$ (2.9 hPa). The SM depicted in Fig. 7b did not exhibit significant variations either over time or between different types of events. In Fig. 7c, LH anomalies were almost symmetrically centered around 0 prior to the occurrence of CDHE, with an average of −0.1 W/m^2; however, they predominantly shifted to positive values during CDHEs, signifying an increase in LH. During $CDHE_d$, the LH anomaly was more pronounced compared to $CDHE_h$, averaging at 3.8 W/m^2 and 2.9 W/m^2, respectively.

Figure 7d and e depict the density distributions of terrestrial and atmospheric coupling index (I_T and I_A) during the pre-CDHE period, CDHE period, and under non-dry-hot conditions. Both prior to and during two kinds of CDHEs, the SM-LH coupling was significantly stronger than under normal conditions. When examining the range >0.3 or less than −0.3 (indicating a relatively strong coupling), the likelihood of I_T falling within this range was 23.4% under non-dry-hot conditions. During the 10-days preceding and during CDHEs, the average probability of I_T falling within this range was 66.7%. During CDHEs, the

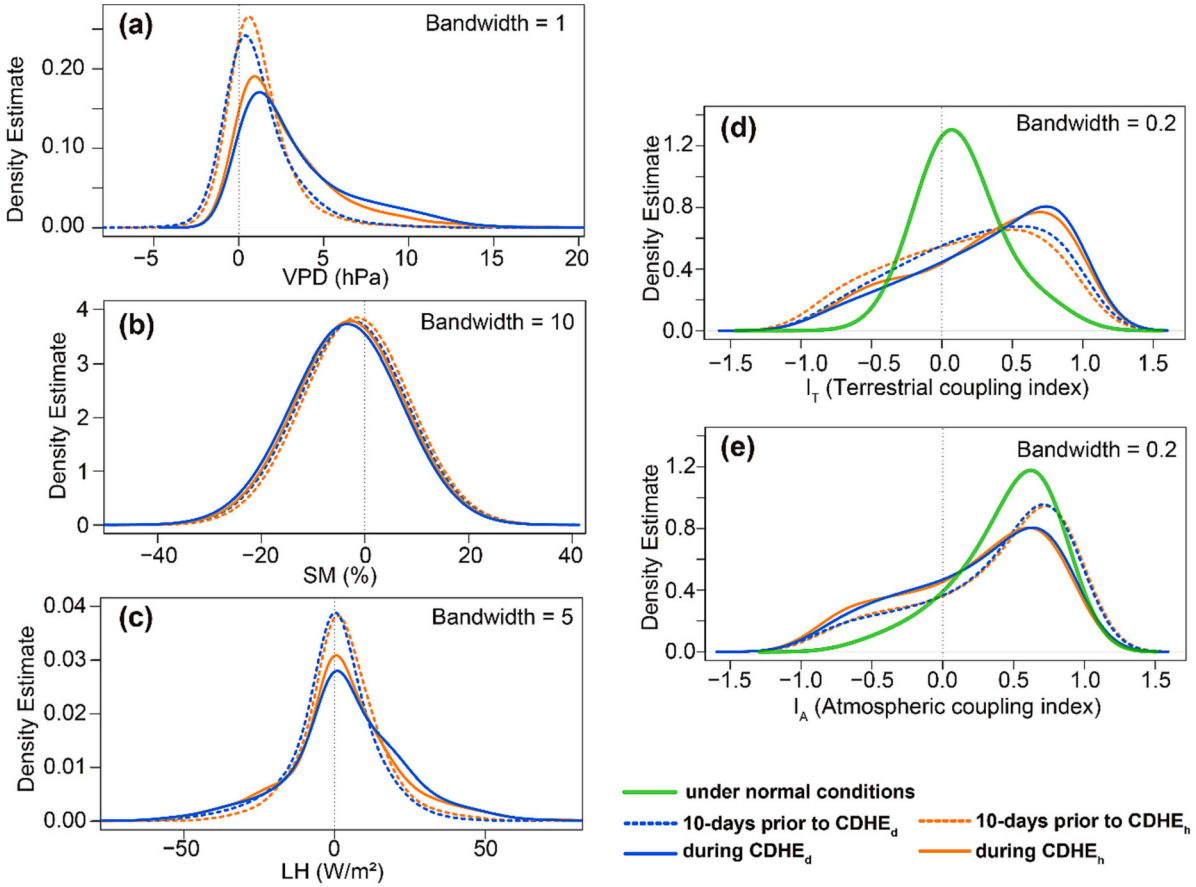

Fig. 7. Kernel density estimates of (a) VPD anomaly, (b) SM anomaly, (c) LH anomaly, (d) terrestrial coupling (SM-LH coupling) index and (e) atmospheric coupling (LH-VPD coupling) index 10-days prior to and during all CDHEs over China from 1961 to 2020, constructed using the gaussian kernel. Orange lines represent $CDHE_h$, and blue lines represent $CDHE_d$. The dashed lines are during the 10 days preceding the events and the solid lines are during the events. Green lines in (d) and (e) indicate the coupling index under non-dry-hot conditions. (For interpretation of the references to colour in this figure legend, the reader is referred to the web version of this article.)

coupling strength ($I_T = 0.34$) increased compared to the 10 days prior to its onset ($I_T = 0.23$). The LH exhibited more negative coupling with SM before the onset of CDHE than after its occurrence (32.5% compared to 25.2%), which signifies that there was a transition of SM-LH coupling from an energy-limited to a water-limited regime. For the LH-VPD coupling, the average I_A under non-dry-hot conditions was 0.45, indicating a positive relation. The proportions of negative LH-VPD coupling (i.e., $I_A < 0$) were higher during the 10-days prior to and the occurrence of CDHE, which averaged 22.8% and 30.5%, respectively, compared to the 11.4% under non-dry-hot conditions.

3.7. The dominant driver of long-term temporal variations of CDHEs

We calculated the correlation between annual P and T over China to examine the long-term relationship between droughts and heatwaves. As shown in Fig. 8a, the annual maximum T and P averaged over China exhibit similar trends and have a positive correlation with a coefficient of 0.51 (at the 0.05 significance level). The grid-based correlation coefficients between annual P and T show that there are more parts that exhibit significant positive relations than those that exhibit negative relations (Fig. 8b). Positively correlated P ~ T account for 57% of the country, and can be found mainly in NW, NE, TP and the lower reaches of the Yangtze River basin. In SW and CN, negative correlations remain prevailing.

Classifying CDHEs into two types ($CDHE_h$ and $CDHE_d$), their annual variations are depicted in Fig. 8c. There is a similarity in the variation patterns of these two types, both of which exhibited a significant increase since the 1990s. To further quantify the contribution of changes in heatwaves and droughts to CDHEs, we conducted the path analysis on their annual frequency over China and in each region, shown in Fig. 8d and e. The direct path coefficient of heatwave on CDHE over China was 0.64 (significant at the 0.01 level), while it was only 0.17 (not significant) for droughts on CDHEs, indicating that changes in CDHE were more related to heatwaves than to droughts. At the regional level, most sub-regions witnessed more contributions from heatwaves than droughts to CDHE changes, with significant and larger direct path coefficients of heatwaves. When comparing the spatial distribution of the trends of heatwave, drought and CDHE in Fig. 5, the northwestern half of Xinjiang and the lower Yangtze River basin showed different patterns with other regions, where CDHEs and droughts decreased significantly while heatwaves increased. Such regional discrepancy was also presented in Fig. 8e, that is, the gaps between the contributions of heatwaves and droughts were smaller in the SW and SE. Furthermore, the R^2 values were generally low in most regions (around 0.3), except for the SW (0.63), suggesting that factors other than droughts and heatwaves, such as their interactions, may also contribute to the long-term variation of CDHEs.

4. Discussion

4.1. Mechanisms triggering the formation of CDHEs

From the perspective of the local land-atmosphere feedback, two main routes can be identified depicting the formation mechanisms of

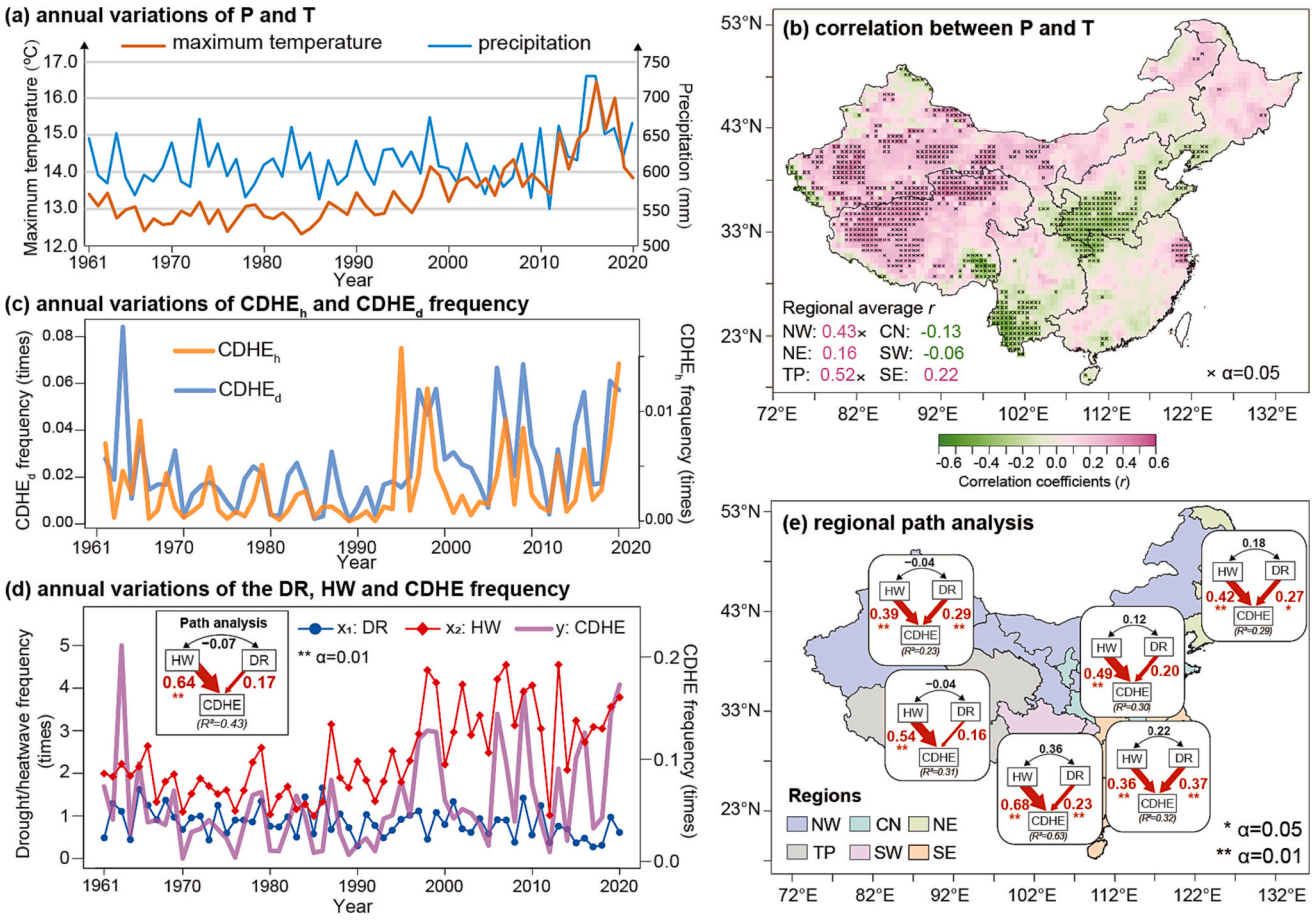

Fig. 8. Relationships between the annual maximum temperature (T) and precipitation (P), and between drought (DR), heatwave (HW) and CDHE frequency. (a) Variations of the annual T and P averaged over China during 1961–2020. (b) Pearson correlations (*r*) between the annual T and P calculated on a grid basis. (c) Variations of the annual frequency of $CDHE_h$ and $CDHE_d$ over China. (d) Variations of the annual frequency of DR, HW and CDHE over China; (e) Regional path analysis of the annual frequency of DR, HW and CDHE; the red arrow denotes the path of contribution, and the number next to it indicates the direct coefficient; the black two-sided arrow and the number represent the Pearson correlation between HW and DR. (For interpretation of the references to colour in this figure legend, the reader is referred to the web version of this article.)

CDHE (see Fig. 9), that is, (a) the orange route, the decrease in precipitation (P) brings about the soil moisture (SM) deficits and the decrease in latent heat flux (LH), hence tending to increase the sensible heat flux and causing the temperature (T) to rise (Gallego-Elvira et al., 2016; Stéfanon et al., 2014; P. Wang et al., 2019a); and (b) the blue route from T to P, which includes two branches, that is: firstly, as the temperature rises, the air becomes drier (with higher vapor pressure deficit, i.e., VPD), which hinders the occurrence of rainfall; and secondly, high temperatures cause an increase of potential evapotranspiration (Ep) and LH, subsequently reduce the SM and LH when the SM is depleted, thus increasing the VPD and leading to precipitation deficits (Vicente-Serrano et al., 2014).

In Section 3.5, we found that CDHEs in China are more likely to occur with droughts occurring before heatwaves, in line with the findings in previous studies (Zhang et al., 2019), and only northern regions of China experienced more CDHEs with heatwaves occurring first. Why a drought mostly precedes a heatwave in the formation of a CDHE is first because the average drought duration in China is more than twice the heatwave duration (see Table 1), consequently, the CDHE has more than twice the opportunity of occurring in a drought than in a heatwave. Secondly, from the perspective of the land-atmosphere feedback, the route from T to P has some seasonal and regional constraints and thus is harder to be achieved: precipitation may be dominated mainly by the moisture availability rather than the moisture storage capacity in cold seasons (characterized by VPD; Berg et al., 2009), thus P is less sensitive to the VPD change and the route T-VPD-P is less effective. In addition, the route T-LH-VPD-P relies on the precondition that the SM has depleted to the "critical value" (Zeppetello et al., 2019). However, in humid regions in southern parts of China, it takes relatively long for the soil to deplete, which makes it harder for this route to take effect after a heatwave. This could be the reason why heatwave-preceded CDHEs mainly occurred in dry northern China (see Fig. 6a). In summary, the local short-term (days to seasons) negative P ~ T correlations controlled by the land-atmosphere interactions played an important role in the formation mechanism of CDHEs, especially in warm seasons when the CDHE is most likely to occur.

Although we classify CDHE into two categories by the occurrence order of drought and heatwave, it does not suggest that the triggering factor of $CDHE_d/CDHE_h$ is only the antecedent dry/hot condition. Large-scale circulation patterns may also result in both high temperature and precipitation deficit and trigger the CDHE, which are more likely to be found in CDHEs with Δd close to 0. Taking the 2019 spring-early summer CDHE over Yunnan province for example, the dry and hot anomalies occurred at very close dates (within 5 days), and subsequently evolved into a typical CDHE, in which the persistent strengthening Western Pacific Subtropical High (WPSH) has been proven to play a crucial role (S. Wang et al., 2019b).

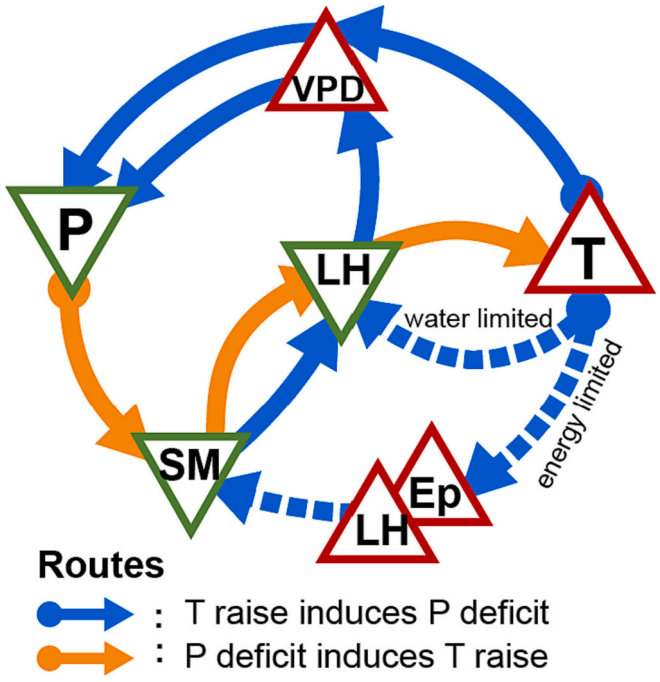

Fig. 9. Simplified formation mechanisms of CDHEs from the perspective of land-atmosphere feedbacks. T, P, SM, LH, Ep and VPD represent temperature, precipitation, soil moisture, latent heat flux, potential evapotranspiration and vapor pressure deficit, respectively. The red triangles indicate variables that increase and the green inverted triangles that decrease. The routes in blue indicate feedback from temperature rising to precipitation deficits, the orange the reverse. The dashed routes are based on local conditions (water-limited regime or energy-limited regime). (For interpretation of the references to colour in this figure legend, the reader is referred to the web version of this article.)

4.2. Heatwaves dominate trends in CDHEs

The negative P ~ T relationships were widely observed in many land regions of the world at the seasonal scale (Berg et al., 2015; Zscheischler and Seneviratne, 2017). However, the long-term variations of P and T in multi-decades tell differently (see Fig. 8a). According to the Clausius-Clapeyron (C—C) equation, every 1 °C temperature increase would lead to a 7% increase in water holding capacity of air, and in the real-world 1% to 3% increase in global precipitation according to observations (Adler et al., 2008). That could be the major physical cause of the long-term positive P ~ T correlation over China, which was in line with the findings of Liu and Wu (2022), and reflected by opposite trends of droughts (decreasing) and heatwaves (increasing) in Fig. 4a and b. Previous studies also showed the overall decrease in drought over China in the past half-century (e.g., Wang et al., 2015) while temperature increased significantly. One important feature that needs to be noticed is the contradiction between the negative P ~ T relationship at the seasonal short temporal scale (see Fig. 2) and the positive P ~ T relationship at the long temporal scale (see Fig. 8) in most regions. The former plays an important role in the onset and formation of CDHE, while the latter is the direct cause of the opposite trends of droughts and heatwaves.

Global warming and heatwaves show strong increasing trends under different warming scenarios (Dosio et al., 2018; Russo et al., 2014). In comparison, precipitation trends are often much weaker and more ambiguous. Bevacqua et al. (2022) stated that precipitation trends would determine future occurrences of compound dry-hot events over land, because local warming would be large enough that future droughts would always coincide with at least moderately hot extremes. While our results show that the variation of heatwaves plays a dominant role in the temporal variation of CDHEs, it should be noted that the warming process may be interrupted by natural variability or human intervention, leading to a temperature drop in a short period, e.g., the period during 1960 to the mid-1980s shown in Fig. 4b-F. During the period from 1960 to the mid-1980s, there was no significant change in the frequency of droughts (Fig. 4a-F), but a significant decrease in the frequency of CDHEs is observed (Fig. 4c-F). Also, the hot thresholds determined by historical behaviors may be obsolete in the future because of human and ecological system adaptations (Wang et al., 2018). Thus, at the long-term scale, we believe that the temporal variation of CDHEs was dominated by the trend of hot extremes rather than droughts.

4.3. Strengths and limitations of CDHId

In Section 3.2, we highlighted the tendency of the joint-probability-based method to excessively identify non-dry or non-hot conditions as CDHE, and demonstrated the effectiveness of the CDHId in excluding those situations. To further analyze the impact of solely relying on the joint probability for CDHE identification, we calculated the proportion of non-dry-hot conditions within CDHEs as identified by the joint probability. When the joint probability remains below a specified threshold for >10 consecutive days, a CDHE is identified. In this section, three representative thresholds (−0.10, 0.05, and 0.02) are selected to identify CDHEs respectively, ranging in severity from severe to mild. Among all identified CDHEs, we calculate the number of days where the daily SPI > -1 or STI < 1 (indicating non-dry or non-hot conditions) and days where SPI > -1 and STI < 1 (neither dry nor hot), as shown in Fig. 10.

Using a threshold of 0.10, the multi-year average duration of CDHEs was 49.8 days, but within these periods, 80% of the days were non-dry or non-hot (SPI > -1 or STI < 1), and an average of 3.6 days were neither dry nor hot (SPI > -1 and STI < 1). When the threshold was raised to 0.05, the multi-year average duration of CDHEs was 22.0 days, with 71.1% of the days being non-dry or non-hot, and 0.09 days being neither dry nor hot. With a threshold of 0.02, the average CDHE duration was 7.7 days, with the proportion of non-dry or non-hot conditions decreasing to 64.4%, averaging 4.9 days. Overall, regardless of the threshold used, identifying CDHE solely based on joint probability results in a considerable proportion of non-dry or non-hot conditions being misidentified as dry-hot conditions. This proportion decreases as the threshold level increases, but even at a joint probability as low as 0.02, more than half of the identified CDHE duration is non-dry or non-hot. Therefore, although an index solely based on joint probability can grade dry-hot conditions, it is important to note that it quantifies the dry-or-hot conditions, rather than the dry-and-hot conditions. The CDHId proposed in our study focuses only on the latter, which is included in the former category but subject to more stringent criteria.

The extreme events were identified at daily resolution in our study, which is less commonly employed in the literature compared to the monthly resolution (Hao et al., 2020; Mazdiyasni and AghaKouchak, 2015; Li et al., 2019). In recent years, with the improvement in the quality and accessibility of daily datasets, along with the more frequent occurrence of sub-monthly scale droughts and heatwaves, there has been an increasing usage of daily resolution when identifying droughts and CDHEs (Li et al., 2021; Wang et al., 2022). Nevertheless, daily indices also have certain limitations, such as being susceptible to short interruptions. During continuous dry-hot days, there may be several days of mild interruption in dry-hot conditions, which might not be sufficient to recover the affected water availability and ecosystems, and thus should not be considered as the end of the CDHE. Daily indices might overlook such discontinuous CDHEs. The method of merging two adjacent CDHEs when the interval between them is relatively small, which is also widely used in drought identification, provides an improvement to this issue. However, determining thresholds for merging two adjacent CDHEs is relatively subjective and needs further analysis and refinement.

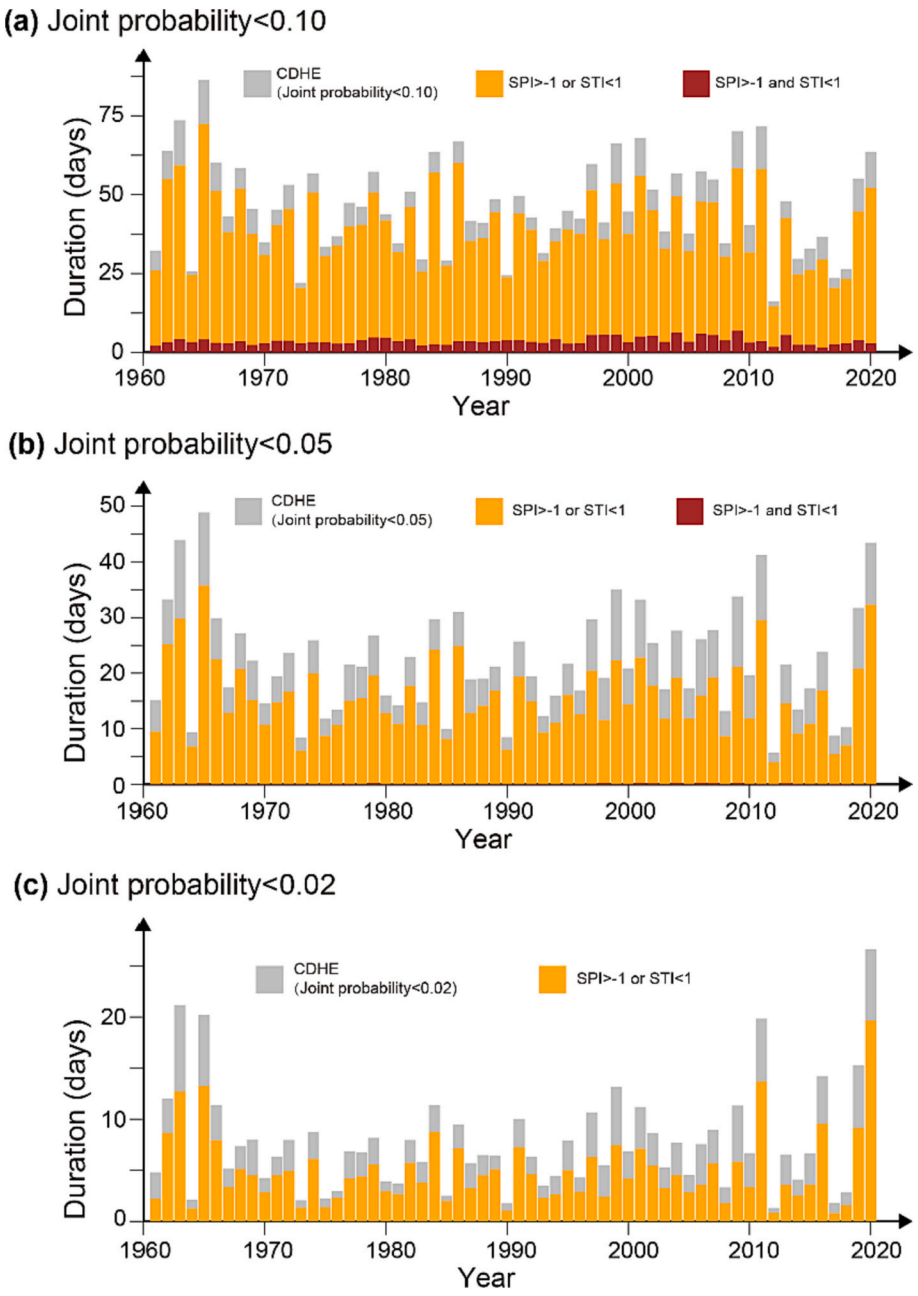

Fig. 10. Interannual variations of CDHE durations identified by the joint cumulative probability of SPI and STI using different thresholds (a. 0.10; b. 0.05; c. 0.02), with a minimal duration of 10 consecutive days. Grey bars represent the CDHE durations; orange bars represent non-dry or non-hot conditions (the daily SPI > -1 or STI < 1) within the identified CDHEs; red bars represent non-dry-hot conditions (the daily SPI > -1 and STI < 1) within CDHEs. (For interpretation of the references to colour in this figure legend, the reader is referred to the web version of this article.)

5. Conclusions

A daily index called CDHId was proposed to identify the compound dry-hot events (CDHEs) in the present study, and the spatiotemporal variations of droughts, heatwaves, and CDHEs in mainland China from 1961 to 2020 were analyzed using standardized precipitation index (SPI), standardized temperature index (STI), and CDHId. CDHEs were classified into two types depending on the onset time difference between the drought and heatwave with each CDHE. Land-atmosphere (L-A) interactions prior to and during two types of CDHEs were investigated using the L-A coupling indices. The dominant factors driving CDHE changes were analyzed by conducting the path analysis between CDHEs and droughts/heatwaves. The results show that:

1. Droughts exhibited a slight decrease in frequency, shortening in duration, and weakening in severity in most parts of mainland China, except for most parts of SW and small parts of southern TP where drought increased significantly. Both heatwaves and CDHEs occurred more frequently after the early 1980s. Northeast China, Southwest China, and the Tibetan Plateau witnessed the most significant rise in CDHEs.
2. From the view of onset and evolution at the short-time scale, CDHEs in China were more likely to be induced by antecedent dry conditions, with 85.2% of CDHEs occurring when the drought preceding heatwave. A stronger L-A coupling than non-dry-hot conditions was observed in both the 10-days before and during the occurrence of CDHEs. With the occurrence of CDHEs, there is a shift in SM-LH

coupling from negative to positive, indicating a transition from an energy-limited regime to a water-limited regime.
3. Although temperature and precipitation present a negative correlation at the seasonal scale, their long-term relationship in multi-decades was positive over China (with a correlation coefficient of 0.51 at the 0.05 significance level). The direct path coefficient of annual heatwave frequency on CDHE frequency over China indicated that the variation of CDHEs in multi-decades was more closely related to heatwaves than to droughts. Overall, the increase in heatwaves dominated the long-term increase of CDHEs in China during 1961–2020.

CRediT authorship contribution statement

Yanjun Hu: Formal analysis, Methodology, Software, Validation, Visualization, Writing – original draft, Writing – review & editing, Data curation. **Wen Wang:** Conceptualization, Funding acquisition, Methodology, Project administration, Supervision, Validation, Writing – review & editing. **Peng Wang:** Supervision, Validation, Writing – review & editing, Resources. **Adriaan J. Teuling:** Supervision, Validation, Writing – review & editing. **Ye Zhu:** Validation, Writing – review & editing.

Declaration of Competing Interest

The authors declare that they have no known competing financial interests or personal relationships that could have appeared to influence the work reported in this paper.

Data availability

The original data sets can be accessed at the National Meteorological Information Center of China Meteorological Administration (http://www.nmic.cn/) and the Institute of Tibetan Plateau Research, Chinese Academy of Sciences (http://www.tpdc.ac.cn). The primary processed data and code can be found at https://github.com/Sugirlstar/CDHEs-in-China.

Acknowledgments

This research was funded by the National Natural Science Foundation of China (No. 41971042 and 41961134003) and the Project on Excellent Post-graduate Dissertation of Hohai University (No. 422003461).

References

Adler, R.F., Gu, G., Wang, J.-J., Huffman, G.J., Curtis, S., Bolvin, D., 2008. Relationships between global precipitation and surface temperature on interannual and longer timescales (1979–2006). J. Geophys. Res. 113, D22104. https://doi.org/10.1029/2008JD010536.

Ben-Ari, T., 2018. Causes and implications of the unforeseen 2016 extreme yield loss in the breadbasket of France. Nat. Commun. 9, 1627. https://doi.org/10.1038/s41467-018-04087-x.

Berg, A., et al., 2015. Interannual Coupling between Summertime Surface Temperature and Precipitation over Land: Processes and Implications for climate Change. J. Clim. 28, 1308. https://doi.org/10.1175/JCLI-D-14-00324.1.

Berg, P., Haerter, J.O., Thejll, P., Piani, C., Hagemann, S., Christensen, J.H., 2009. Seasonal characteristics of the relationship between daily precipitation intensity and surface temperature. J. Geophys. Res. Atmos. 114 https://doi.org/10.1029/2009JD012008.

Bevacqua, E., Zappa, G., Lehner, F., Zscheischler, J., 2022. Precipitation trends determine future occurrences of compound hot–dry events. Nat. Clim. Chang. 12, 350–355. https://doi.org/10.1038/s41558-022-01309-5.

Brás, T.A., Seixas, J., Carvalhais, N., Jägermeyr, J., 2021. Severity of drought and heatwave crop losses tripled over the last five decades in Europe. Environ. Res. Lett. 16, 065012 https://doi.org/10.1088/1748-9326/abf004.

Budyko, M.I., 1961. The heat balance of the Earth's surface. Sov. Geogr. 2, 3–13. https://doi.org/10.1080/00385417.1961.10770761.

Chen, Y., Yang, K., He, J., Qin, J., Shi, J., Du, J., He, Q., 2011. Improving land surface temperature modeling for dry land of China. J. Geophys. Res. Atmos. 116 https://doi.org/10.1029/2011JD015921.

Ding, T., Ke, Z., 2015. Characteristics and changes of regional wet and dry heat wave events in China during 1960–2013. Theor. Appl. Climatol. 122, 651–665. https://doi.org/10.1007/s00704-014-1322-9.

Dirmeyer, P.A., Jin, Y., Singh, B., Yan, X., 2013. Trends in land–atmosphere interactions from CMIP5 simulations. J. Hydrometeorol. 14, 829–849. https://doi.org/10.1175/JHM-D-12-0107.1.

Dosio, A., Mentaschi, L., Fischer, E.M., Wyser, K., 2018. Extreme heat waves under 1.5 °C and 2 °C global warming. Environ. Res. Lett. 13, 054006 https://doi.org/10.1088/1748-9326/aab827.

Feng, Y., Liu, W., Sun, F., Wang, H., 2021. Changes of compound hot and dry extremes on different land surface conditions in China during 1957–2018. Int. J. Climatol. 41 https://doi.org/10.1002/joc.6755.

Gallego-Elvira, B., Taylor, C.M., Harris, P.P., Ghent, D., Veal, K.L., Folwell, S.S., 2016. Global observational diagnosis of soil moisture control on the land surface energy balance. Geophys. Res. Lett. 43, 2623–2631. https://doi.org/10.1002/2016GL068178.

Ganguli, P., Reddy, M.J., 2013. Probabilistic assessment of flood risks using trivariate copulas. Theor. Appl. Climatol. 111, 341–360. https://doi.org/10.1007/s00704-012-0664-4.

Han, S., Tian, F., Hu, H., 2014. Positive or negative correlation between actual and potential evaporation? Evaluating using a nonlinear complementary relationship model. Water Resour. Res. 50, 1322–1336. https://doi.org/10.1002/2013WR014151.

Hao, Z., Hao, F., Singh, V.P., Zhang, X., 2018. Quantifying the relationship between compound dry and hot events and El Niño–southern Oscillation (ENSO) at the global scale. J. Hydrometeorol. 567, 332–338. https://doi.org/10.1016/j.jhydrol.2018.10.022.

Hao, Z., Hao, F., Singh, V.P., Ouyang, W., Zhang, X., Zhang, S., 2020. A joint extreme index for compound droughts and hot extremes. Theor. Appl. Climatol. 142, 321–328. https://doi.org/10.1007/s00704-020-03317-x.

He, Y., Fang, J., Xu, W., Shi, P., 2022. Substantial increase of compound droughts and heatwaves in wheat growing seasons worldwide. Int. J. Climatol. 42, 5038–5054. https://doi.org/10.1002/joc.7518.

Hirsch, A.L., Evans, J.P., Di Virgilio, G., Perkins-Kirkpatrick, S.E., Argüeso, D., Pitman, A. J., Carouge, C.C., Kala, J., Andrys, J., Petrelli, P., Rockel, B., 2019. Amplification of Australian heatwaves via local land-atmosphere coupling. J. Geophys. Res. Atmos. 124, 13625–13647. https://doi.org/10.1029/2019JD030665.

Hsu, H., Dirmeyer, P.A., 2022. Deconstructing the soil moisture–latent heat flux relationship: the range of coupling regimes experienced and the presence of nonlinearity within the sensitive Regime. J. Hydrometeorol. 23, 1041–1057. https://doi.org/10.1175/JHM-D-21-0224.1.

Kendall, M.G., 1955. Rank Correlation Methods, 2nd ed. Charles Griffin and Company, p. 196.

Li, J., Wang, Z., Wu, X., Zscheischler, J., Guo, S., Chen, X., 2021. A standardized index for assessing sub-monthly compound dry and hot conditions with application in China. Hydrol. Earth Syst. Sci. 25, 1587–1601. https://doi.org/10.5194/hess-25-1587-2021.

Li, X., You, Q., Ren, G., Wang, S., Zhang, Y., Yang, J., Zheng, G., 2019. Concurrent droughts and hot extremes in Northwest China from 1961 to 2017. Int. J. Climatol. 39, 2186–2196. https://doi.org/10.1002/joc.5944.

Libonati, R., et al., 2022. Assessing the role of compound drought and heatwave events on unprecedented 2020 wildfires in the Pantanal. Environ. Res. Lett. 17, 015005 https://doi.org/10.1088/1748-9326/ac462e.

Liu, Z., Wu, G., 2022. Quantifying the precipitation–temperature relationship in China during 1961–2018. Int. J. Climatol. 42, 2656–2669. https://doi.org/10.1002/joc.7384.

Mann, H.B., 1945. Nonparametric Tests against Trend. Econometrica. 13, 245–259. https://doi.org/10.2307/1907187.

Mazdiyasni, O., AghaKouchak, A., 2015. Substantial increase in concurrent droughts and heatwaves in the United States. PNAS. 112, 11484–11489. https://doi.org/10.1073/pnas.1422945112.

McKee, T.B., Doesken, N.J., Kleist, J., 1995. Drought monitoring with multiple time scales. In: Proc. Ninth Conf. On Applied Climatology. Amer. Meteor. Soc, Dallas, TX, pp. 233–236.

Miralles, D.G., Gentine, P., Seneviratne, S.I., Teuling, A.J., 2019. Land–atmospheric feedbacks during droughts and heatwaves: state of the science and current challenges. Ann. N. Y. Acad. Sci. 1436, 19–35. https://doi.org/10.1111/nyas.13912.

Mo, K.C., Lettenmaier, D.P., 2015. Heat wave flash droughts in decline. Geophys. Res. Lett. 42, 2823–2829. https://doi.org/10.1002/2015GL064018.

Muñoz-Sabater, J., Dutra, E., Agustí-Panareda, A., Albergel, C., Arduini, G., Balsamo, G., Boussetta, S., Choulga, M., Harrigan, S., Hersbach, H., Martens, B., Miralles, D.G., Piles, M., Rodríguez-Fernández, N.J., Zsoter, E., Buontempo, C., Thépaut, J.-N., 2021. ERA5-Land: a state-of-the-art global reanalysis dataset for land applications. Earth Syst. Sci. Data 13, 4349–4383. https://doi.org/10.5194/essd-13-4349-2021.

Nagler, T., Schepsmeier, U., Stoeber, J., Brechmann, E.C., Graeler, B., Erhardt, T., 2021. VineCopula: Statistical Inference of Vine Copulas. R package version 2.4.3. URL. https://CRAN.R-project.org/package=VineCopula.

National Meteorological Information Center, 2012. Dataset of Gridded Daily Precipitation in China, version 2.0. China Meteorological Administration. URL. http://www.nmic.cn/ (accessed 4.10.21).

Osman, M., Zaitchik, B.F., Winstead, N.S., 2022. Cascading Drought-Heat dynamics during the 2021 Southwest United States Heatwave. Geophys. Res. Lett. 49 https://doi.org/10.1029/2022GL099265 e2022GL099265.

Otkin, J.A., Svoboda, M., Hunt, E.D., Ford, T.W., Anderson, M.C., Hain, C., Basara, J.B., 2018. Flash droughts: a review and assessment of the challenges imposed by rapid-

onset droughts in the United States. B. Am. Meteorol. Soc. 99, 911–919. https://doi.org/10.1175/BAMS-D-17-0149.1.
Perkins, S.E., Alexander, L.V., 2013. On the Measurement of Heat Waves. J. Clim. 26, 4500–4517. https://doi.org/10.1175/JCLI-D-12-00383.1.
Rosseel, Y., 2012. Lavaan: an R package for structural equation modeling. J. Stat. Softw. 48, 1–36. https://doi.org/10.18637/jss.v048.i02.
Ruffault, J., Curt, T., Moron, V., Trigo, R.M., Mouillot, F., Koutsias, N., Pimont, F., Martin-StPaul, N., Barbero, R., Dupuy, J.-L., Russo, A., Belhadj-Khedher, C., 2020. Increased likelihood of heat-induced large wildfires in the Mediterranean Basin. Sci. Rep. 10, 13790. https://doi.org/10.1038/s41598-020-70069-z.
Russo, S., et al., 2014. Magnitude of extreme heat waves in present climate and their projection in a warming world. J. Geophys. Res. Atmos. 119 (12), 500–512. https://doi.org/10.1002/2014JD022098.
Seo, Y.-W., Ha, K.-J., 2022. Changes in land-atmosphere coupling increase compound drought and heatwaves over northern East Asia. npj Clim. Atmos. Sci. 5, 1–9. https://doi.org/10.1038/s41612-022-00325-8.
Shi, C.X., Jiang, L.P., Zhang, T., 2014. Status and plans of CMA land data assimilation system (CLDAS) project. Geophys. Res. Abstr. 16. EGU2014–5671. http://meetingorganizer.copernicus.org/EGU2014/EGU2014-5671.pdf.
Stagge, J.H., Tallaksen, L.M., Gudmundsson, L., Van Loon, A.F., Stahl, K., 2015. Candidate Distributions for Climatological Drought Indices (SPI and SPEI). Int. J. Climatol. 35, 4027–4040. https://doi.org/10.1002/joc.4267.
Stéfanon, M., Drobinski, P., D'Andrea, F., Lebeaupin-Brossier, C., Bastin, S., 2014. Soil moisture-temperature feedbacks at meso-scale during summer heat waves over Western Europe. Clim. Dyn. 42, 1309–1324. https://doi.org/10.1007/s00382-013-1794-9.
Teuling, A.J., Seneviratne, S.I., Williams, C., Troch, P.A., 2006. Observed timescales of evapotranspiration response to soil moisture. Geophys. Res. Lett. 33 https://doi.org/10.1029/2006GL028178.
Tomé, A.R., Miranda, P.M.A., 2004. Piecewise linear fitting and trend changing points of climate parameters. Geophys. Res. Lett. 31, L02207. https://doi.org/10.1029/2003GL019100.
Vicente-Serrano, S.M., et al., 2014. Evidence of increasing drought severity caused by temperature rise in southern Europe. Environ. Res. Lett. 9, 044001 https://doi.org/10.1088/1748-9326/9/4/044001.
Vogel, J., Paton, E., Aich, V., Bronstert, A., 2021. Increasing compound warm spells and droughts in the Mediterranean Basin. Wea. Climate Extrem. 32, 100312 https://doi.org/10.1016/j.wace.2021.100312.
Wang, P., Li, D., Liao, W., Rigden, A., Wang, W., 2019a. Contrasting evaporative responses of ecosystems to heatwaves traced to the opposing roles of vapor pressure deficit and surface resistance. Water Resour. Res. https://doi.org/10.1029/2019WR024771, 2019WR024771.
Wang, Q., Zhang, R., Qi, J., Zeng, J., Wu, J., Shui, W., Wu, X., Li, J., 2022. An improved daily standardized precipitation index dataset for mainland China from 1961 to 2018. Sci. Data. 9, 124. https://doi.org/10.1038/s41597-022-01201-z.
Wang, S., Yuan, X., Wu, R., 2019b. Attribution of the persistent spring–summer hot and dry extremes over Northeast China in 2017. Bull. Am. Meteorol. Soc. 100, S85–S89. https://doi.org/10.1175/BAMS-D-18-0120.1.
Wang, W., Zhu, Y., Xu, R., Liu, J., 2015. Drought severity change in China during 1961–2012 indicated by SPI and SPEI. Nat. Hazards 75, 2437–2451. https://doi.org/10.1007/s11069-014-1436-5.
Wang, W., Wang, J., Romanowicz, R., 2021. Uncertainty in SPI calculation and its impact on drought assessment in different climate Regions over China. J. Hydrometeorol. 22, 1369–1383. https://doi.org/10.1175/JHM-D-20-0256.1.
Wang, Y., Nordio, F., Nairn, J., Zanobetti, A., Schwartz, J.D., 2018. Accounting for adaptation and intensity in projecting heat wave-related mortality. Environ. Res. 161, 464–471. https://doi.org/10.1016/j.envres.2017.11.049.
Wu, X., Hao, Z., Hao, F., Li, C., Zhang, X., 2019. Spatial and temporal variations of compound droughts and hot extremes in China. Atmosphere. 10, 95. https://doi.org/10.3390/atmos10020095.
Xie, W., Zhou, B., You, Q., Zhang, Y., Ullah, S., 2020. Observed changes in heat waves with different severities in China during 1961–2015. Theor. Appl. Climatol. 141, 1529–1540. https://doi.org/10.1007/s00704-020-03285-2.
Yang, K., He, J., 2016. China Meteorological Forcing Dataset (1979–2015). National Tibetan Plateau Data Center. https://doi.org/10.3972/westdc.002.2014.db. URL. (accessed 5.20.21).
Ye, L., Shi, K., Xin, Z., Wang, C., Zhang, C., 2019. Compound droughts and heat waves in China. Sustainability. 11, 3270. https://doi.org/10.3390/su11123270.
Yu, R., Zhai, P., 2020. More frequent and widespread persistent compound drought and heat event observed in China. Sci. Rep. 10, 14576. https://doi.org/10.1038/s41598-020-71312-3.
Yuan, X., Wang, Y., Ji, P., Wu, P., Sheffield, J., Otkin, J.A., 2023. A global transition to flash droughts under climate change. Science. 380, 187–191. https://doi.org/10.1126/science.abn6301.
Zeppetello, L.R.V., Battisti, D.S., Baker, M.B., 2019. The Origin of Soil Moisture Evaporation "Regimes". J. Clim. 32, 6939–6960. https://doi.org/10.1175/JCLI-D-19-0209.1.
Zhang, Q., She, D., Zhang, L., Wang, G., Chen, J., Hao, Z., 2022. High sensitivity of compound drought and heatwave events to global warming in the future. Earth's Future 10. https://doi.org/10.1029/2022EF002833 e2022EF002833.
Zhang, W., Luo, M., Gao, S., Chen, W., Hari, V., Khouakhi, A., 2021. Compound hydrometeorological extremes: drivers, mechanisms and methods. Front. Earth Sci. 9, 941. https://doi.org/10.3389/feart.2021.673495.
Zhang, Y., You, Q., Mao, G., Chen, C., Ye, Z., 2019. Short-term concurrent drought and heatwave frequency with 1.5 and 2.0 °C global warming in humid subtropical basins: a case study in the Gan River Basin, China. Clim. Dyn. 52, 4621–4641. https://doi.org/10.1007/s00382-018-4398-6.
Zscheischler, J., Seneviratne, S.I., 2017. Dependence of drivers affects risks associated with compound events. Sci. Adv. 3, e1700263 https://doi.org/10.1126/sciadv.1700263.
Zscheischler, J., et al., 2014. Impact of large-scale climate extremes on biospheric carbon fluxes: an intercomparison based on MsTMIP data. Glob. Biogeochem. Cycles 28, 585–600. https://doi.org/10.1002/2014GB004826.
Zscheischler, J., et al., 2018. Future climate risk from compound events. Nat. Clim. Chang. 8, 469–477. https://doi.org/10.1038/s41558-018-0156-3.